Articles

Solution Structure of the 30 kDa Polysulfide-Sulfur Transferase Homodimer from *Wolinella succinogenes*[†,‡]

Yi-Jan Lin,[§,||] Felician Dancea,[§,||] Frank Löhr,[§] Oliver Klimmek,[⊥] Stefania Pfeiffer-Marek,[§,@] Michael Nilges,[#] Hans Wienk,[§,+] Achim Kröger,[⊥,○] and Heinz Rüterjans*[,§]

Institute of Biophysical Chemistry, Center for Biomolecular Magnetic Resonance, J. W. Goethe-University, Marie-Curie-Strasse 9, D-60439 Frankfurt am Main, Germany, Institute of Microbiology, J. W. Goethe-University, Marie-Curie-Strasse 9, D-60439 Frankfurt am Main, Germany, and Unit of Structural Bio-informatics, Pasteur Institute, 25-28 rue du Dr Roux, F-75724 Paris CEDEX 15, France

Received September 15, 2003; Revised Manuscript Received December 5, 2003

ABSTRACT: The periplasmic polysulfide-sulfur transferase (Sud) protein encoded by *Wolinella succinogenes* is involved in oxidative phosphorylation with polysulfide-sulfur as a terminal electron acceptor. The polysulfide-sulfur is covalently bound to the catalytic Cys residue of the Sud protein and transferred to the active site of the membranous polysulfide reductase. The solution structure of the homodimeric Sud protein has been determined using heteronuclear multidimensional NMR techniques. The structure is based on NOE-derived distance restraints, backbone hydrogen bonds, and torsion angle restraints as well as residual dipolar coupling restraints for a refinement of the relative orientation of the monomer units. The monomer structure consists of a five-stranded parallel β-sheet enclosing a hydrophobic core, a two-stranded antiparallel β-sheet, and six α-helices. The dimer fold is stabilized by hydrophobic residues and ion pairs found in the contact area between the two monomers. Similar to rhodanese enzymes, Sud catalyzes the transfer of the polysulfide-sulfur to the artificial acceptor cyanide. Despite their similar functions and active sites, the amino acid sequences and structures of these proteins are quite different.

The periplasmic polysulfide-sulfur transferase (Sud)[1] protein is induced in the anaerobic Gram-negative bacterium *Wolinella succinogenes* when it grows with formate and polysulfide as catabolic substrates (*1*, *2*) and has been previously proposed to serve as a polysulfide binding and transferase protein (*3*), allowing rapid polysulfide-sulfur reduction at low polysulfide concentrations. The Sud protein is comprised of two identical subunits of ~15 kDa and does not contain prosthetic groups or heavy metal ions. Each monomer contains a single cysteine residue, which was found to be essential for the protein function. *In vitro*, it appears that each cysteine covalently binds up to 10 polysulfide-sulfur (S_n^{2-}) atoms, when incubated in a polysulfide solution (*4*). Sud is thought to transfer polysulfide-sulfur to the catalytic molybdenum ion located at the periplasmic active site of the membrane protein polysulfide reductase (*5*). The transfer of the polysulfide-sulfur from Sud to polysulfide reductase probably occurs in a complex of the two proteins, when a sulfur atom is reductively cleaved from the polysulfide chain (*4*).

A BLAST search (*6*) pointed out that the primary sequence of Sud is only slightly homologous to those of other proteins with known three-dimensional structure (Figure 1). The homologous partners are sulfur transferase or rhodanese enzymes that catalyze the transfer of a sulfur atom from suitable donors to nucleophilic acceptors (e.g., from thiosulfate to cyanide). Their three-dimensional structures display a typical α/β topology and have a similar environment in the active site primarily with respect to the main chain conformation of the Cys-located active site loop. The highest level of primary sequence similarity (30% identical residues) is observed

[†] Financial support from the Deutsche Forschungsgemeinschaft (SFB472) and from the Frankfurt University Center of Biomolecular Magnetic Resonance is gratefully acknowledged. H.W. acknowledges receipt of a fellowship from the Alexander-von-Humboldt Foundation.

[‡] The coordinates of the polysulfide-sulfur transferase homodimer from *W. succinogenes* have been deposited in the RCSB Protein Data Bank as entry 1QXN.

* To whom correspondence should be addressed: Institute of Biophysical Chemistry, Biozentrum, N230, Marie-Curie-Str. 9, D-60439 Frankfurt am Main, Germany. Phone: +49-(0)69-798-29622. Fax: +49-(0)69-798-29632. E-mail: hruet@bpc.uni-frankfurt.de.

[§] Institute of Biophysical Chemistry, Center for Biomolecular Magnetic Resonance, J. W. Goethe-University.

[||] These authors made equal contributions to this study.

[⊥] Institute of Microbiology, J. W. Goethe-University.

[@] Present address: Computational Chemistry and Molecular Modelling, Aventis Pharma Deutschaland GmbH, D-65926 Frankfurt am Main, Germany.

[#] Pasteur Institute.

[+] Present address: Department of NMR Spectroscopy, Bijvoet Center for Biomolecular Research, Utrecht University, Padualaan 8, 3584 CH Utrecht, The Netherlands.

[○] Deceased June 11, 2002.

[1] Abbreviations: Sud, polysulfide-sulfur transferase (formerly sulfide dehydrogenase); NMR, nuclear magnetic resonance; NOE, nuclear Overhauser effect; NOESY, nuclear Overhauser enhancement and exchange spectroscopy; ADR, ambiguous distance restraints; RDC or D^{NH}, residual dipolar coupling; rmsd, root-mean-square deviation.

10.1021/bi0356597 CCC: $27.50
Published on Web 01/21/2004

```
Sud     1   ADMGEKFDATFKA...QVKAAKADMVMLSPKDAYKLLQENPDITLID. 44
GlpE    11  ..............................DAHQKLQEK.EAVLVD. 25
Rhobov 154 ATLNRSLLKTYEQVLENLESKRFQLVDSRAQGRYLGTQPEPDAVGLDS 201
RhdA   133 APAGGPVALSLHD...EPTASR.DYLLGRLGAA........DLAIWD. 167
                                                        *

Sud    45  ..VRDPDE......LKAMGK..PDVKNYKHMS..........RGKLEP 72
GlpE   26  ..IRDPQS......F.AMGH..A.VQAF.HLT..........NDTLGA 50
Rhobov 202 GHIRGSVN......MPFMNF..LTEDGFEK.S..........PEELRA 230
RhdA   168 ..ARSPQEYRGEKVLAAKGGHIPGAVNFEWTAAMDPSRALRIRTDIAG 213
              *

Sud    73  LLAKSGLDPEKPVVVFCKTAARAALAGKTLREYGFKTIYNSEGGMDKW 120
GlpE   51  FMRDNDFD..TPVMVMCYHGNSSKGAAQYLLQQGYDVVYSIDGGFEAW 96
Rhobov 231 MFEAKKVDLTKPLIATCRKGVTA.......................... 253
RhdA   214 RLEELGITPDKEIVTHCQTHHRSGLTYLIAKALGYPRVKGYAGSWGEW 261
                          *
```

FIGURE 1: Multiple-amino acid sequence alignment of rhodanese-like proteins with known three-dimensional structures: Sud, *E. coli* GlpE (*7*), bovine liver rhodanese (*37*), and *A. vinelandii* rhodanese (*8*). The primary sequence of Sud was taken to be the reference, and the pair alignments were obtained with BLAST. The active site loop residues are shown in red and the additional charged residues in the active site of Sud in blue. Invariant residues are marked with asterisks.

between Sud and *Escherichia coli* GlpE, a protein that has been proposed to have the prototype structure for the ubiquitous single-domain rhodanese module (*7*). With regard to the amino acid composition and the location of charged residues in the active site region, the best match is observed between Sud and rhodanese of *Azobacter vinelandii* (*8*), despite a lower level of sequence homology (23% identical residues).

In this paper, we present the solution structure determination of the Sud homodimer from *W. succinogenes*. The backbone chemical shift assignment was previously reported (*9*). Within the NMR spectra of homodimers, all symmetry-related nuclei have equivalent magnetic environments and therefore are degenerated in chemical shift. The symmetry degeneracy simplifies the resonance assignment problem (only half of the nuclei must be assigned), but hampers considerably the NOESY assignment and structure calculations, mainly because it is not possible *a priori* to distinguish between the intramonomer, intermonomer, and comonomer (mixed) NOE cross-peaks. There are two ways to overcome the symmetry degeneracy problem of the NOESY data: the use of asymmetric labeling experiments to distinguish between intra- and intermolecular NOEs and/or special structure calculation methods that are able to deal with the inherent ambiguity of the NOE-derived distance restraints. For the structure calculations presented here, we used the symmetry ADR method (*10*) in combination with data from asymmetric labeling experiments.

MATERIALS AND METHODS

Sample Preparation and NMR Experiments. The expression and purification of the Sud protein were carried out using a protocol similar to that previously described (*3*), including a C-terminal His tag of six residues. Uniform ^{15}N or ^{15}N and ^{13}C labeling was performed by growing bacteria on isotope-enriched minimal medium using [^{15}N]ammonium chloride (Martek) and $^{13}C_3$-enriched glycerol (Martek) as the main nitrogen and carbon sources, respectively. For protein samples labeled with ^{2}H, ^{15}N, and ^{13}C, the bacteria were grown on Celtone-dCN (Martek, deuteration degree of 97%). NMR samples of the purified protein (0.6−1.2 mM dimer) were prepared in 50 mM sodium phosphate (pH 7.6), 1 mM polysulfide (S_n^{2-}), 13 mM sulfide, and 5% (v/v) D_2O. The protein was loaded with sulfur before being transferred to the buffer solution described above. To exclude oxygen from the NMR probes, the sample tubes were flushed with nitrogen while being filled and tightly sealed afterward. Under these conditions, it can be assumed that the protein remains sulfur-loaded during the NMR experiments.

Unless stated otherwise, the NMR data were acquired at 300 K using Bruker DMX-600 and DRX-800 NMR spectrometers equipped with xyz-gradient ^{1}H, ^{15}N, ^{13}C triple-resonance probe heads. The sensitivity and resolution of the triple-resonance experiments were improved by employing the TROSY technology (*11*, *12*). The software packages XWINNMR, AURELIA (Bruker Analytische Messtechnik GmbH, Karlsruhe, Germany), and NMRPipe (*13*) were used for data processing and data analysis. The ^{1}H chemical shifts were referenced to internal DSS (2,2-dimethyl-2-silapentane-5-sulfonate sodium salt), while the ^{15}N and ^{13}C chemical shifts were calibrated indirectly using the appropriate gyromagnetic ratios (*14*).

The ^{13}C side chain assignments for ^{2}H-, ^{13}C-, and ^{15}N-labeled Sud were based on three-dimensional (3D) CC(CO)NH (*15*) and CC(CA)NH (*16*) experiments with ^{13}C spin lock times of 21 and 17 ms, respectively. The $^{1}H_\alpha$ chemical shifts were obtained from a 3D HCACO experiment, and the ^{1}H side chain resonances were assigned using 3D H(C)CH-COSY and H(C)CH-TOCSY experiments with a ^{13}C spin lock time of 17 ms on a uniformly ^{15}N- and ^{13}C-labeled protein. The aromatic proton resonances were obtained via a two-dimensional (2D) NOESY experiment with a mixing time of 70 ms, a 2D TOCSY experiment with an unlabeled sample in D_2O with a ^{1}H spin lock time of 44 ms, and a 3D ^{13}C-separated NOESY-HSQC experiment with a mixing time of 70 ms employing a constant time $^{13}C-^{1}H$ TROSY evolution period (*17*) optimized for aromatic carbons on a ^{15}N- and ^{13}C-labeled sample in H_2O.

The stereospecific assignments for the isopropyl groups of Val and Leu residues were determined using a biosynthetic approach (*18*) on the basis of the $^{13}C-^{13}C$ one-bond couplings within 2D ^{13}C HSQC and 2D constant time ^{13}C HSQC experiments on a 10% ^{13}C-labeled sample.

The NOE assignments and distance restraints for NH−NH correlations were obtained from a four-dimensional (4D) $^{15}N/^{15}N$-separated NOESY experiment (*19*, *20*) with a mixing time of 300 ms on uniformly ^{2}H- and ^{15}N-labeled protein in H_2O. Further NOE data were collected from a 3D ^{13}C-separated NOESY-HSQC with a mixing time of 80 ms using a

uniformly ^{13}C- and ^{15}N-labeled protein in D_2O, a 3D ^{15}N-separated NOESY-HSQC experiment with a mixing time of 75 ms recorded with a uniformly ^{15}N-labeled protein in H_2O, a 3D constant time methyl ^{13}C-separated NOESY-HSQC experiment with a mixing time of 100 ms on a uniformly ^{13}C- and ^{15}N-labeled protein in H_2O, and a 2D NOESY experiment with a mixing time of 70 ms on an unlabeled sample in D_2O.

The asymmetrically labeled samples used for the measurement of the intermonomer NOEs were prepared from unlabeled and ^{2}H- and $^{15}N(^{13}C)$-labeled Sud−His_6 dimers. They were mixed in equal amounts at a very low concentration (each species at 10 nM) in an anaerobic buffer containing 50 mM potassium phosphate and 10% (v/v) glycerol (pH 8.0). To induce the monomerization of the isolated dimers, 0.02% (w/v) sodium dodecyl sulfate was added. The mixture was stirred for 48 h at room temperature under anaerobic conditions. For the dimerization initiation and protein recovery, the whole mixture was applied to a 10 mL Ni−nitrilotriacetic agarose (Qiagen) column equilibrated with 50 mM potassium phosphate and 10% (v/v) glycerol (pH 8.0). The column was extensively rinsed with the same buffer (0.5 L) for removal of the SDS, and then the protein was eluted with this buffer containing 0.2 M imidazole. The eluted Sud protein was concentrated up to 30 g/L by pressure dialysis using a 10 kDa filter, and the imidazole was removed by repeated dilution and concentration (five times) of the protein with a buffer containing 50 mM potassium phosphate (pH 7.65).

To determine NOEs across the dimer interface, a 3D ^{15}N-separated NOESY-HSQC experiment with a mixing time of 120 ms on a heterodimer sample containing one ^{2}H- and ^{15}N-labeled monomer and one unlabeled monomer (*21*) and a 4D constant time *J*-resolved ^{13}C-separated NOESY experiment (*22*) with a mixing time of 150 ms on a sample containing one ^{13}C-labeled monomer and one unlabeled monomer were carried out. The former experiment yields intermonomer NOEs between the amide protons of the ^{2}H- and ^{15}N-labeled and the carbon-bound protons of the unlabeled species. The latter one allows the separation of inter- and intramolecular NOEs along the *J*-resolved dimension in which the intramolecular NOEs between ^{13}C-bound protons appear at $\pm J_{CH}/2$ Hz, while intermolecular NOEs between ^{13}C- and ^{12}C-bound protons appear at a frequency offset of zero because they are not *J*-modulated.

The slowly exchanging amide protons were identified by recording 2D $^{1}H-^{15}N$ HSQC experiments, 1 day and 5 days after the transfer of the protein into a D_2O solution. This information combined with the strong HN−Hα connectivities within and between different β-strands allows the identification of the β-strands and of the hydrogen bonds between β-strands. The amide protons located in the internal five-stranded parallel β-sheet remain unexchanged 5 days after the addition of D_2O. The backbone amide protons involved in hydrogen bonding were also measured using an $^{h3}J_{NCO}$ TROSY-NHCO experiment (*23*).

For the residual dipolar coupling measurements, the isotropic sample contained 0.55 mM dimeric protein in 50 mM sodium phosphate (pH 7.6), 1 mM polysulfide (S_n^{2-}), 13 mM sulfide, and 10% (v/v) D_2O, while the anisotropic one had 0.48 mM protein in the same buffer with the C8E5/*n*-octanol alignment medium (*24*). The molar ratio of C8E5 to *n*-octanol was 0.87, and the C8E5/water ratio was 6% (w/v). A generalized version of the $^{15}N-^{1}H$ TROSY experiment (*11*, *25*, *26*) was used for the measurement of $^{1}J_{NH}$ couplings and $^{1}J_{NH} + D^{NH}$ couplings on a nonoriented and oriented sample, respectively. The residual dipolar coupling values (RDC, D^{NH}) were calculated from the coupling differences between the $^{1}J_{NH} + D^{NH}$ couplings and the $^{1}J_{NH}$ scalar couplings.

Structure Calculation and NOE Assignment. NOESY cross-peak volumes were determined using the Bruker AURELIA program and converted into distance restraints using the symmetry ADR (ambiguous distance restraint) protocol described by Nilges (*27*), which accounts for the ambiguity in the NOEs arising from dispersion and symmetry degeneracy. The experimental unambiguous intermonomer NOEs and the NH−NH NOE assignments derived from the 4D $^{15}N/^{15}N$-separated NOESY experiment were used as 6 Å upper and 2 Å lower bounds, respectively. The hydrogen bond restraints were defined as 1.8−2.3 Å for the H−O distance and 2.8−3.3 Å for the N−O distance.

The TALOS program (*28*) was used to predict the backbone torsion angle intervals from the amino acid sequence and chemical shift information. The tolerance of ϕ and ψ angles was set to ± 2 standard deviations (SD) for all the dihedral angle constraints.

NMR studies of homodimers are problematic because of the difficulty in distinguishing between intra-, inter-, and comonomer (mixed) NOE correlations. We used the symmetry ADR protocols of ARIA for an iterative structure calculation and NOE assignment (*10*, *29*). The symmetry ADRs describe the ambiguity of NOE peaks arising from both symmetry and dispersion degeneracy by computing a "d^{-6} summed distance" over all pairs of protons that are possible assignments for a particular cross-peak, including the intra- and intermonomer contributions. To enforce the 2-fold symmetry, the conformational target function contains two special pseudoenergy terms: a noncrystallographic symmetry (NCS) restraint (*30*) and a distance symmetry (DSYM) restraint potential (*27*). The former serves to minimize the atomic rms deviation between the two monomers, thus making the two monomers identical, while the latter forces the two monomers into a symmetrical arrangement.

The NOE assignment was performed in nine iterations using the ARIA scheme (*31*), where a generation of structures is used for the NOE analysis (calibration, partial assignment, and noise removal) of the following one. We calculated 50 structures per iteration (60 in the last iteration), the best 30% of the models being used for the refinement of the next ones. The starting conformers were constructed using the hydrogen bonding information and manually assigned NOEs from the 4D $^{15}N/^{15}N$-separated NOESY and NOESY experiments on the asymmetrically labeled dimers as well as the TALOS prediction for dihedral angles. The RDC data were used starting with the third iteration and having a rather low weighting factor. For the determination of the alignment tensor parameters (axial component and rhombicity), we analyzed the "powder pattern" of the RDC distribution (*32*). After the iterative NOE assignment was completed, the weight of the target function RDC term was tuned within several turns of structure calculations such that the agreement between the observed and back-calculated values of the

residual dipolar couplings was supposed to be similar to the experimental error.

To assess the reliability of the automatic assignment output, a collection of MATLAB routines were developed (data not shown) for proof of the consistency between the NOE assignment table and the 3D ^{15}N- and ^{13}C-edited NOESY spectra by looking at the cross-peak symmetry within the spectra. If we neglect the spin diffusion, every HN−HN NOE must appear twice in a ^{15}N-resolved NOESY spectrum. The same type of symmetry should be present in ^{13}C-resolved and between ^{15}N- and ^{13}C-resolved NOESY spectra when different heteroatoms are involved. All the NOE assignments, which are not supported by other cross-peaks between the corresponding residues and which have no symmetry partners, were manually verified.

The structures were calculated using a simulated annealing protocol comprising four stages: (I) a high-temperature torsion angle dynamics phase at 10 000 K (2200 MD steps), (II) a torsion angle cooling stage from 10 000 to 2000 K (2200 steps), (III) a Cartesian dynamics cooling stage from 2000 to 1000 K (20 000 steps), and (IV) a second Cartesian dynamics cooling stage from 1000 to 50 K (18 000 steps). All non-stereospecifically assigned prochiral groups, except the manually assigned isopropyl groups, were treated with a floating chirality approach (*33*). The polysulfide-binding Sud structure was calculated by assuming a Cys residue containing five polysulfide-sulfur atoms. The polysulfide tail topology was derived using X-ray data (*34*). Since there is no structural information available for the polysulfide from NMR, the orientation of the sulfur chain has been derived from steric considerations. The final structures were calculated with an *ab initio* simulated annealing protocol starting from a random monomer structure with good local geometry, the dimer being generated by a duplication of the monomer unit followed by a 180° rotation around one of its internal axes and a 60 Å translation in the same dimension. Thus, the starting monomer orientation possesses the correct 2-fold symmetry, which is completely unbiased due to the explicit inter- and intramonomer NOE assignments performed in an iterative manner. To account for the electrostatic interactions between the side chains of the ionic residues (44 per monomer not including the His tag) and to prevent the unrealistic packing that might result from a simple repulsive representation of the nonbonding energy term, the final structures were refined in explicit solvent (water) using a special force field for electrostatic and van der Waals interactions (*35*). The symmetry restraint terms were deliberately left out at this final stage to allow small deviations from the ideal 2-fold symmetry and therefore will better represent the internal dynamics within the homodimer. The 10 lowest-energy structures out of 100 calculated structures were refined in water. All the structural representations of the protein were drawn with MOLMOL (*36*).

RESULTS AND DISCUSSION

Chemical Shifts and NOE Assignments. Using the known backbone chemical shifts (*9*) as a starting point, the majority of side chain ^{1}H and ^{13}C resonances were assigned by a combination of 3D CC(CO)NH, CC(CA)NH, H(C)CH-COSY, and H(C)CH-TOCSY experiments. Altogether, ~74% of the resonances were assigned. Stereospecific assignments of nearly all isopropyl groups of Val and Leu residues were obtained (with a single exception, Leu73).

Table 1: Structural Statistics for the 10 Lowest-Energy Simulated, Annealed, and Water-Refined Structures of the Sud Homodimer

no. of unambiguous NOE distance restraints	4182
sequential ($\|i - j\| = 1$)	1115
medium-range ($1 < \|i - j\| < 5$)	605
long-range ($\|i - j\| > 4$)	830
intermonomer	102
no. of ambiguous NOE distance restraints	1095
comonomer	142
no. of H-bond restraints	22
no. of dihedral angle restraints	340
no. of RDC restraints	162
rms deviation for distance restraints[a] (Å)	0.014 ± 0.001
rms deviation for angle restraints[a] (deg)	0.509 ± 0.016
rms deviation for RDC restraints[a] (Hz)	1.043 ± 0.039
rms deviation for covalent geometry[a]	
bond lengths (Å)	0.0034 ± 0.0001
bond angles (deg)	0.507 ± 0.0154
impropers (deg)	1.335 ± 0.057
Ramachandran plot[b]	
most allowed regions	86.3%
disallowed regions	0.6%
rmsd of the NMR ensemble (Å)[c]	
monomer core backbone	0.81 ± 0.18
dimer backbone	0.96 ± 0.20

[a] Evaluated with CNS/ARIA. [b] Calculated with PROCHECK-NMR (*38*). [c] Mean global backbone rmsd calculated with MOLMOL. The flexible loop between residues 89 and 94 was not used for rmsd calculations.

A total of 8 (16 considering the symmetry-related ones) intermonomer NOEs were unambiguously assigned using asymmetric labeling experiments (see Materials and Methods). Because of the low concentration of the asymmetrically labeled dimers in the NMR sample, only few intermonomer NOEs could be determined. On the basis of these experiments, the contact regions between the two monomers were found to involve mainly residues F7, D8, T10, and F11 of one monomer and A75 and Y105 of the other monomer.

From 9532 experimental NOESY peaks (2D homonuclear and 3D ^{15}N- and ^{13}C-edited NOESYs), 1095 ambiguous and 3758 unambiguous nonredundant NOE-derived distance restraints were obtained, including 86 intermonomer and 142 comonomer NOEs. This structural data together with 340 predefined ϕ and ψ angle constraints, 402 backbone−backbone and backbone−side chain NH−NH distance restraints derived from the 4D ^{15}N/^{15}N-separated NOESY, 22 hydrogen bonds between the β-strands, 16 experimental intermonomer NOEs (asymmetric labeling), and 162 amide residual dipolar couplings were used for the final structure calculations (see Table 1 for a detailed structural statistics).

Comparison between the Structures Calculated with and without Residual Dipolar Coupling Restraints. Figure 2 shows the backbone atoms for the Sud structure calculated with and without residual dipolar coupling restraints. The relative orientation of the two monomers was significantly improved by the residual dipolar coupling restraints, the RDC-refined dimer structure showing a more compact form than the RDC-free one. The mean backbone rmsd of the NMR ensembles drops from 1.64 to 0.96 Å for the RDC-refined conformers considering the whole dimer, although the monomer cores (without the α-helical N-terminus) were equally well-defined, having a value of ~0.8 Å in both cases. For the rmsd calculations, the segment between residues 89

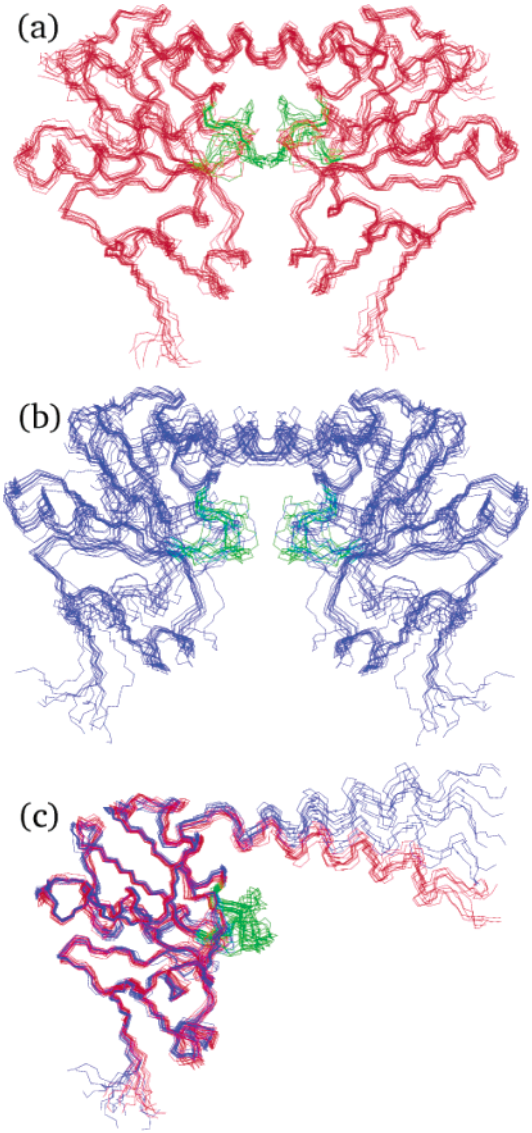

FIGURE 2: (a) Backbone plot of the 10 best RDC-refined structures of the Sud dimer. (b) Backbone plot of the RDC-free NMR ensemble (10 models) of Sud. (c) Backbone representation of the monomer cores (residues 25−130) superimposed for the RDC-refined (red) and RDC-free (blue) structures of the Sud protein. The flexible loop (residues 89−94) is colored green.

and 94 was not considered, which is poorly defined because of the lack of experimental data. If the monomer structures in the two ensembles are compared, the core regions are nearly superimposable, the main difference resulting from the relative orientation of the monomer units dictated by different positioning of the N-terminal α-helix. The secondary structure elements are also similar. The result clearly illustrates that the residual dipolar coupling restraints improve the definition of the domain relative orientation for multimodular proteins.

Description of the Structure. Figure 3 shows the ribbon representations of the solution structure of the Sud homodimer. The monomer unit has an α/β topology with six α-helices (helices I−VI) packed against a central core of five parallel β-strands (βA, βB, and βD−βF) and a lateral two-stranded antiparallel β-sheet (βC and βG) which may be involved in the structural stabilization of the C-terminal segment. For the minimized average structure, the β-strands were formed by residues 23−25 (βA), 41−44 (βB), 56 and

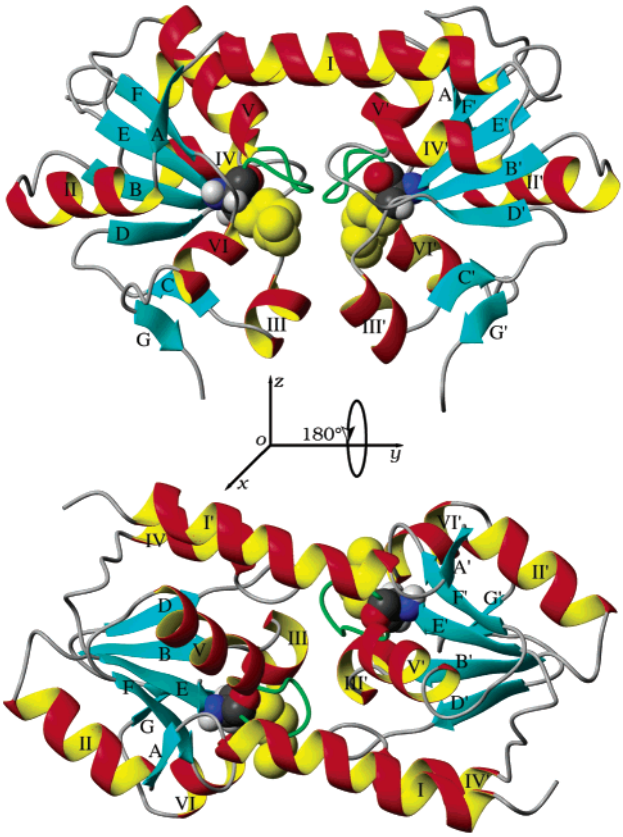

FIGURE 3: Ribbon representations of the Sud dimer. The catalytic cysteines (with a five-atom polysulfide chain attached) are depicted using a CPK model. The 2-fold symmetry axes are the *OZ* and *OX* axes for the top and bottom structures, respectively. The active site loop (residues 89−94) is colored green.

57 (βC), 62−64 (βD), 85−88 (βE), 110−113 (βF), and 127 and 128 (βG) within each subunit, while the helices are observed for residues 4−20 (I), 27−36 (II), 48−53 (III), 71−77 (IV), 95−103 (V), and 117−122 (VI). The polysulfide chains bound to the cysteine residues are pointing in opposite directions, to the outside of the protein. The distance between the two S_δ atoms of cysteine residues ranges from 16.7 to 18.9 Å. The N-terminal helices (I and I′) of the two monomers are oriented parallel to each other, but rather distant in space; therefore, an interaction between them is unlikely. Helix I of one monomer unit interacts with helices IV′ and V′ of the second unit to form a three-helix bundle stabilizing the dimeric structure.

On the basis of the intermonomer NOEs assigned with ARIA, the residues participating in the interaction between the two monomers are mainly F7, F11, and V15, located at the hydrophobic side of helix I with partners L74′, A75′, L79′, L97′, and Y105′ in the opposite unit. Hence, mainly hydrophobic interactions are involved in stabilizing the dimeric structure. For example, the aromatic side chains of F7 and F11 interact with Y105′ and the methyl groups of L74′, while F11 and V15 interact with L97′. Because of the interactions with aromatic rings, the H_δ resonances of L74 and L79 are shifted to a higher field by values between 0.1 and 0.2 ppm. A salt bridge in this region between K12 (helix I) and E71′ (helix IV′) may form, since the side chains move within 5 Å of each other.

Structure−Function Relationship. Sud serves as a polysulfide-sulfur binding and transfer protein, transferring the

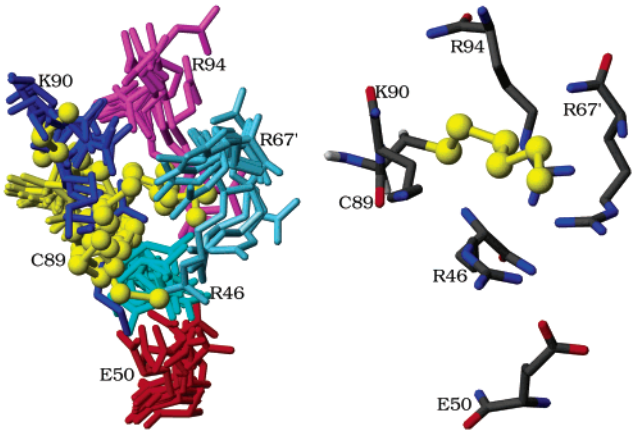

FIGURE 4: Positively charged polysulfide binding pocket. Because of the lack of resonance assignments, the side chains conformation is poorly defined. The left side of the plot represents a superposition of the NMR ensemble (10 models) of the Sud dimer structure, while the right side represents the minimized average conformer of the ensemble.

aqueous polysulfide to the active site of polysulfide reductase, which is exposed to the periplasmic side of the cytoplasmic membrane of *W. succinogenes*. The two identical subunits of Sud, each with a single cysteine residue, covalently bind two polysulfide chains with up to 10 sulfur atoms. Using site-directed mutagenesis, it was shown that the cysteine residues are essential for the sulfur binding and transferase activity of Sud (*4*).

The active site environment of Sud resembles that of rhodanese of *A. vinelandii* (RhdA), in both cases the catalytic cysteine residues being located at the bottom of shallow round pockets close to the interdomain boundary, at the beginning of a loop with a cradle-like conformation that is connecting a central β-strand with an interface α-helix. RhdA is a covalently bound multidomain protein consisting of two similar but not identical α/β domains at the N-terminal and C-terminal domain. Unlike Sud which has a polysulfide binding site in each monomer unit, RhdA has a single functional cysteine residue located in the C-terminal domain. Side chains in the intermonomer contact area around the active site of Sud indicate that formation of the dimer is required for the protein function. The active site cysteine is the first residue of loop 89−94, connecting strand βE to helix V (Figure 3). Because of the lack of chemical shift assignments (both backbone and side chain resonances could not be assigned, except the HN−N and $H_\alpha-C_\alpha$ resonances of C89 and the $H_\alpha-C_\alpha$ resonance of T91), this segment is poorly defined, which may be a result of multiple conformations induced by the polysulfide mobility. In a similar way, resonances of R46 and R67, both located near the sulfur tail, were not assigned presumably to such a conformational heterogeneity and mobility. The Sud structure reveals a positively charged binding pocket for the negative polysulfide-sulfur chain formed by residues R46, R67′ (adjacent monomer unit), K90, and R94 (Figure 4). An electrostatic binding pocket that partially covers the Sud-polysulfide tail is consistent with previous MALDI mass spectroscopy investigations, which indicated a much lower dissociation constant for the first two sulfur atoms of the polysulfide chain (*4*). The positively charged side chains of R46, R67′, K90, and R94 of Sud interact with and stabilize the first two S−S bonds of the negatively charged polysulfide, while the negatively charged side chain of E50 interacts with R46 (Figure 4). The mutation of any of the above-mentioned residues leads to a loss of the sulfur transferase activity (data not published). The amino acid sequence alignment of RhdA and Sud indicates that R46, E50, R67, C89, and R94 (Sud numbering) are conserved residues (Figure 1).

CONCLUSIONS

The active site loop surrounding the catalytic cysteine (preserved in all rhodanese enzymes) appears to be flexible for the Sud protein as evidenced by the missing chemical shift assignments of the related residues (residues 89−94). The polysulfide tail extends out of a positively charged binding pocket (residues R46, R67′, K90, and R94), where Sud may contact the polysulfide reductase. The determination of the precise functional roles of these residues in the mechanism of the transfer of the polysulfide-sulfur from Sud to the active site polysulfide reductase remains an interesting goal for future studies.

REFERENCES

1. Klimmek, O., Kröger, A., Steudel, R., and Holdt, G. (1991) *Arch. Microbiol. 155*, 177−182.
2. Kreis-Kleinschmidt, V., Fahrenholz, F., Kojro, E., and Kröger, A. (1995) *Eur. J. Biochem. 227*, 137−142.
3. Klimmek, O., Kreis, V., Klein, C., Simon, J., Wittershagen, A., and Kröger, A. (1998) *Eur. J. Biochem. 253*, 263−269.
4. Klimmek, O., Stein, T., Pisa, R., Simon, J., and Kröger, A. (1999) *Eur. J. Biochem. 263*, 79−84.
5. Prisner, T., Lyubenova, S., Atabay, Y., MacMillan, F., Kröger, A., and Klimmek, O. (2003) *J. Biol. Inorg. Chem. 8*, 419−426.
6. Altschul, S. F., Madden, T. L., Schaffer, A. A., Zhang, J., Zhang, Z., Miller, W., and Lipman, D. J. (1997) *Nucleic Acids Res. 25*, 3389−3402.
7. Spallarossa, A., Donahue, J. L., Larson, T. J., Bolognesi, M., and Bordo, D. (2001) *Structure 9*, 1117−1125.
8. Bordo, D., Deriu, D., Colnaghi, R., Carpen, A., Pagani, S., and Bolognesi, M. (2000) *J. Mol. Biol. 298*, 691−704.
9. Lin, Y. J., Pfeiffer, S., Löhr, F., Klimmek, O., and Rüterjans, H. (2000) *J. Biomol. NMR 18*, 285−286.
10. O'Donoghue, S. I., and Nilges, M. (1999) *Biol. Magn. Reson. 17*, 131−161.
11. Pervushin, K., Riek, R., Wider, G., and Wüthrich, K. (1997) *Proc. Natl. Acad. Sci. U.S.A. 94*, 12366−12371.
12. Salzmann, M., Wider, G., Pervushin, K., Senn, H., and Wüthrich, K. (1999) *J. Am. Chem. Soc. 121*, 844−848.
13. Delaglio, F., Grzesiek, S., Vuister, G. W., Zhu, G., Pfeifer, J., and Bax, A. (1995) *J. Biomol. NMR 6*, 277−293.
14. Wishart, D. S., Bigam, C. G., Yao, J., Abildgaard, F., Dyson, H. J., Oldfield, E., Markley, J. L., and Sykes, B. D. (1995) *J. Biomol. NMR 6*, 135−140.
15. Farmer, B. T., and Venters, R. A. (1995) *J. Am. Chem. Soc. 117*, 4187−4188.
16. Löhr, F., and Rüterjans, H. (2002) *J. Magn. Reson. 156*, 10−18.
17. Pervushin, K., Riek, R., Wider, G., and Wüthrich, K. (1998) *J. Am. Chem. Soc. 120*, 6394−6400.
18. Neri, D., Szyperski, T., Otting, G., Senn, H., and Wüthrich, K. (1989) *Biochemistry 28*, 7510−7516.
19. Venters, R. A., Metzler, W. J., Spicer, L. D., Mueller, L., and Farmer, B. T. (1995) *J. Am. Chem. Soc. 117*, 9592−9593.
20. Grzesiek, S., Wingfield, P., Stahl, S., Kaufman, J. D., and Bax, A. (1995) *J. Am. Chem. Soc. 117*, 9594−9595.
21. Ferentz, A. E., Opperman, T., Walker, G. C., and Wagner, G. (1997) *Nat. Struct. Biol. 4*, 979−983.
22. Melacini, G. (2000) *J. Am. Chem. Soc. 122*, 9735−9738.
23. Wang, Y. X., Jacob, J., Cordier, F., Wingfield, P., Stahl, S. J., Lee-Huang, S., Torchia, D., Grzesiek, S., and Bax, A. (1999) *J. Biomol. NMR 14*, 181−184.
24. Rückert, M., and Otting, G. (2000) *J. Am. Chem. Soc. 122*, 7793−7797.

25. Andersson, P., Annila, A., and Otting, G. (1998) *J. Magn. Reson. 133*, 364−367.
26. Lerche, M. H., Meissner, A., Poulsen, F. M., and Sørensen, O. W. (1999) *J. Magn. Reson. 140*, 259−263.
27. Nilges, M. (1993) *Proteins 17*, 297−309.
28. Cornilescu, G., Delaglio, F., and Bax, A. (1999) *J. Biomol. NMR 13*, 289−302.
29. Nilges, M., and O'Donoghue, S. I. (1998) *Prog. NMR Spectrosc. 32*, 107−139.
30. Brünger, A. T., Adams, P. D., Clore, G. M., DeLano, W. L., Gros, P., Grosse-Kunstleve, R. W., Jiang, J. S., Kuszewski, J., Nilges, M., Pannu, N. S., Read, R. J., Rice, L. M., Simonson, T., and Warren, G. L. (1998) *Acta Crystallogr. D54* (Part 5), 905−921.
31. Linge, J. P., O'Donoghue, S. I., and Nilges, M. (2001) *Methods Enzymol. 339*, 71−90.
32. Clore, G. M., Gronenborn, A. M., and Bax, A. (1998) *J. Magn. Reson. 133*, 216−221.
33. Folmer, R. H., Hilbers, C. W., Konings, R. N., and Nilges, M. (1997) *J. Biomol. NMR 9*, 245−258.
34. Steudel, R., Pridohl, M., Buschmann, J., and Luger, P. (1995) *Chem. Ber. 128*, 725−728.
35. Linge, J. P., and Nilges, M. (1999) *J. Biomol. NMR 13*, 51−59.
36. Koradi, R., Billeter, M., and Wüthrich, K. (1996) *J. Mol. Graphics 14*, 51−55.
37. Ploegman, J. H., Drent, G., Kalk, K. H., Hol, W. G., Heinrikson, R. L., Keim, P., Weng, L., and Russell, J. (1978) *Nature 273*, 124−129.
38. Laskowski, R. A., Rullmannn, J. A., MacArthur, M. W., Kaptein, R., and Thornton, J. M. (1996) *J. Biomol. NMR 8*, 477−486.

BI0356597